



RESEARCH LETTER

10.1002/2015GL063819

Key Points:

- Coseismic and postseismic deformation observation after the 2012 earthquakes
- Explanation of postseismic GPS motion and gravity change
- Dominant viscoelastic relaxation after the strike-slip earthquake

Supporting Information:

- Figures S1 and S2

Correspondence to:

S.-C. Han,
shin-chan.han@newcastle.edu.au

Citation:

Han, S.-C., J. Sauber, and F. Pollitz (2015), Coseismic compression/dilatation and viscoelastic uplift/subsidence following the 2012 Indian Ocean earthquakes quantified from satellite gravity observations, *Geophys. Res. Lett.*, *42*, 3764–3772, doi:10.1002/2015GL063819.

Received 11 MAR 2015

Accepted 23 APR 2015

Accepted article online 28 APR 2015

Published online 19 MAY 2015

Coseismic compression/dilatation and viscoelastic uplift/subsidence following the 2012 Indian Ocean earthquakes quantified from satellite gravity observations

Shin-Chan Han¹, Jeanne Sauber², and Fred Pollitz³

¹School of Engineering, University of Newcastle, Callaghan, New South Wales, Australia, ²Planetary Geodynamics Laboratory, NASA Goddard Space Flight Center, Greenbelt, Maryland, USA, ³U.S. Geological Survey, Menlo Park, California, USA

Abstract The 2012 Indian Ocean earthquake sequence (M_w 8.6, 8.2) is a rare example of great strike-slip earthquakes in an intraoceanic setting. With over a decade of Gravity Recovery and Climate Experiment (GRACE) data, we were able to measure and model the unanticipated large coseismic and postseismic gravity changes of these events. Using the approach of normal mode decomposition and spatial localization, we computed the gravity changes corresponding to five moment tensor components. Our analysis revealed that the gravity changes are produced predominantly by coseismic compression and dilatation within the oceanic crust and upper mantle and by postseismic vertical motion. Our results suggest that the postseismic positive gravity and the postseismic uplift measured with GPS within the coseismic compressional quadrant are best fit by ongoing uplift associated with viscoelastic mantle relaxation. Our study demonstrates that the GRACE data are suitable for analyzing strike-slip earthquakes as small as M_w 8.2 with the noise characteristics of this region.

1. Introduction

The M_w 8.6 Indian Ocean earthquake of 11 April 2012 occurred ~100–300 km west of the Sunda megathrust (Figure 1). This earthquake was part of a sequence of large strike-slip earthquakes that started with a M_w 7.2 foreshock 3 months before the M_w 8.6 main shock, and it was followed by a M_w 8.2 aftershock 2 h afterward [e.g., Duputel *et al.*, 2012]. Seismic data analysis found tens of meters of slips were released mostly within the upper 40 km in 100 s but with slip extending to depths of 60 km, unusually deep for earthquakes within the oceanic lithosphere [Wei *et al.*, 2013; McGuire and Beroza, 2012; Hill *et al.*, 2015]. The transient, dynamic stressing from this large, high-stress drop event caused a short-term increase in global seismicity rates at magnitudes $4.5 < M_w < 7.0$ [Pollitz *et al.*, 2012, 2014].

This sequence of strike-slip events followed the M_w 9.2 2004 Sumatra-Andaman and M_w 8.6 2005 Nias-Simeulue earthquakes located along the Sunda subduction zone. Coulomb stress calculations show that thrust faulting associated with these great earthquakes favors slip on outer-rise strike-slip faults that are oblique to the trench [Rollins and Stein, 2010; Meng *et al.*, 2012]. Additionally, the timing of the strike-slip sequence may have been modulated by postseismic stress buildup associated with viscoelastic relaxation following the 2004–2005 great earthquakes [Delescluse *et al.*, 2012].

The coseismic and postseismic surface deformation associated with the 2012 strike-slip events has been measured with GPS, such as Sumatran GPS Array (SuGAR) network; however, the GPS sites are only at distant locations in northern Sumatra (>300 km) and additionally due to the proximity to the Sunda megathrust may include deformation due to other nearby processes.

The gravitational potential changes for this event have been also measured through changes of instantaneous relative motions of two Gravity Recovery and Climate Experiment (GRACE) satellites coorbiting around 500 km altitude [Han *et al.*, 2013]. We used the time series of monthly GRACE solutions of the global gravity fields processed by optimizing the signals over the Indian ocean earthquake region to document the gravity change prior to, during, and following these large oceanic strike-slip events. We examined the gravity data to understand the coseismic and postseismic deformation by contrasting seafloor

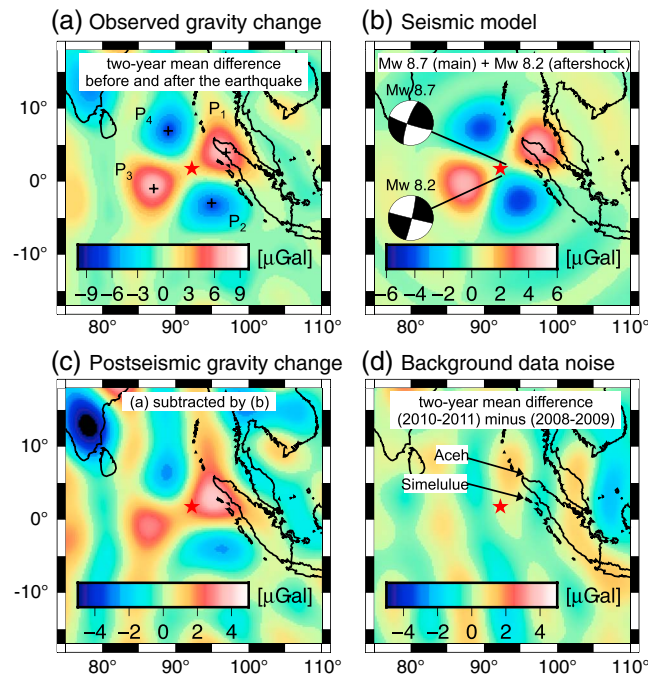


Figure 1. (a) The GRACE observed gravity change due to the 2012 Indian Ocean earthquakes is computed by differencing the 2 year mean field before and after the earthquake. (b) The synthetic gravity change caused by the coseismic deformation is computed using a seismic finite fault model. (c) The postseismic GRACE gravity change is computed by subtracting the seismic model prediction shown in Figure 1b from the mean difference field shown in Figure 1. (d) The same as Figure 1a but during the two years between 2010–2011 and 2008–2009 inferring the background noise level of the GRACE mean fields (including the postseismic gravity signals after 2004 Sumatra-Andaman rupture).

smoothing or any a posteriori filter applied. The positive gravity change up to 6 μGal (P_1) or larger was found around the Aceh region and the Simeulue island, and the same size of gravity change is found southwest of the epicenter in the middle of the Indian Ocean (P_3). The negative gravity change with the same magnitude is also found northwest (P_4) and southeast (P_2) of the epicenter. It was anticipated that no significant vertical motion would result, and thus no significant gravity change, after any strike-slip event. However, the GRACE data demonstrated the first-ever measurement of gravity change after strike-slip earthquakes as featured in Figure 1a. In the following sections, we elaborate on the detailed processes responsible for such gravity change during the coseismic and postseismic period.

Figure 1b presents the coseismic gravity change computed using the seismic finite fault model of the M_w 8.6 main rupture from Yue *et al.* [2012] and the centroid moment tensor solution of the M_w 8.2 aftershock from Duputel *et al.* [2012]. The effect of the ocean interacting with the seafloor motion was considered. The gravity change from the aftershock is about 20% of that from the main shock. The spatial patterns of the aftershock and the main shock are nearly identical at the resolution of this study. The gravity change computed from the finite fault model of Wei *et al.* [2013] is different by less than 1 μGal .

The difference between the observed and synthetic coseismic gravity fields, that is shown in Figure 1c, presents a similar spatial pattern to the seismic model but with a reduced amplitude by $\sim 50\%$ (or $\pm 3 \mu\text{Gal}$). Yue *et al.* [2012], Duputel *et al.* [2012], and Wei *et al.* [2013] reported $1.2\text{--}1.3 \times 10^{22} \text{ N m}$ of the moment release from the M_w 8.6 main shock and Duputel *et al.* [2012] and Wei *et al.* [2013] found $0.2\text{--}0.3 \times 10^{22} \text{ N m}$ from the M_w 8.2 aftershock. The total moment of $1.4\text{--}1.6 \times 10^{22} \text{ N m}$ was released and responsible for the gravity change as depicted in Figure 1b. Nearly 50% of the gravity difference ($\sim 0.7\text{--}0.8 \times 10^{22} \text{ N m}$) as shown in Figure 1c is too large to be associated with the uncertainty of the seismic fault models. It is also

vertical motion and compression and dilatation involved with the horizontal motion of the faults. We tested viscoelastic relaxation models with a series of alternate rheological structures against the observed postseismic gravity change to constrain the rheological response of the oceanic lithosphere and asthenosphere. Finally, our results were compared independently with some of the GPS vertical motion measurements in northern Sumatra.

2. GRACE Gravity Observations

We computed the average gravity changes over 2 years after the earthquakes from June 2012 to June 2014 with respect to the mean field from April 2010 to March 2012, using the monthly solutions of global gravity fields (Level 2 products) processed by University of Texas Center for Space Research [Tapley *et al.*, 2004]. The GRACE gravity solution was not available for the month of May 2012 due to lack of accelerometer measurements. Figure 1a presents the observed gravity change of the coseismic and postseismic deformation, computed at the spatial resolution of 500 km (spherical harmonic degree and order up to 40) without

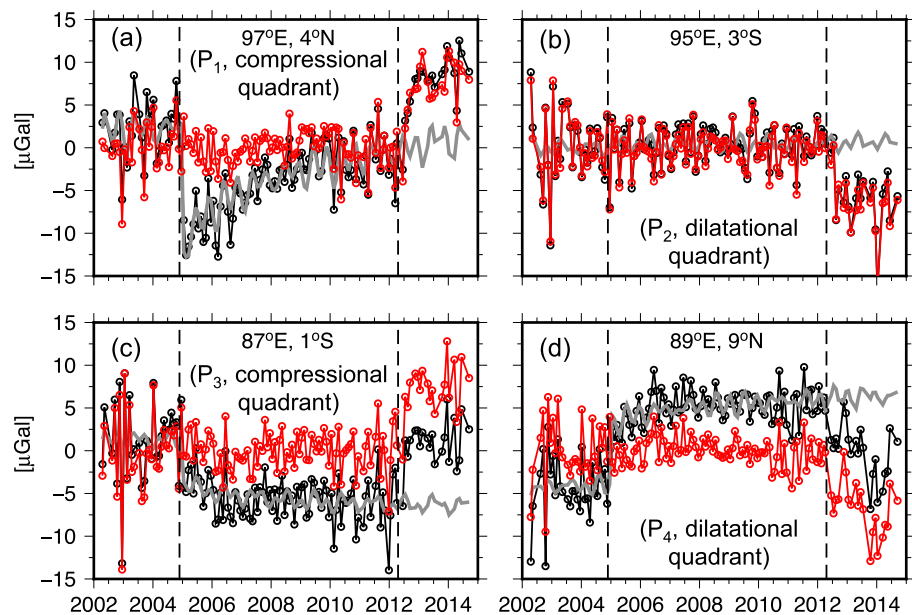


Figure 2. Time series of the GRACE gravity measurements at four locations, at the center of the two compressional and two dilatational quadrants. The exact location is marked with the black cross symbol in Figure 1a. The black and gray line indicates the GRACE data and the data fit of the seasonal change and coseismic and postseismic change of the 2004 Sumatra-Andaman earthquake, respectively. The red line is the residual data (black minus gray) that retains the gravity change associated only with the great 2012 earthquake.

larger than the GRACE data noise as inferred by the mean difference during the years with no great earthquake (Figure 1d). Therefore, we assert it is related to postseismic processes.

The monthly time series of the GRACE gravity data were examined at four distinct locations at the compressional (P_1 and P_3) and dilatational (P_2 and P_4) quadrants. Figure 2 shows the GRACE monthly gravity values evaluated at each location of P_1 through P_4 (black lines with circles), the data fit (gray lines), and the residuals (red lines with circles). The GRACE data before the 2012 Indian Ocean earthquakes were used to calculate the data fit using parameters such as seasonal sinusoids (for climate signals), 161 day sinusoids (for S_2 ocean tide), Heaviside step (for the 2004 Sumatra-Andaman earthquake), and logarithmic function (for the postseismic deformation after the 2004 earthquake). Then the data fit was extrapolated to the entire GRACE data to compute the residuals shown with red colored lines. This process effectively removes the majority of the signals not associated with the 2012 Indian Ocean earthquake, including the coseismic and postseismic effects of the 2004 Sumatra-Andaman earthquake. The coseismic gravity increase and decrease were clearly observed in association with the 2012 earthquakes at the compressional (P_1 and P_3) and dilatational (P_2 and P_4) quadrants, respectively. However, the gravity data evaluated at each point location is too noisy to quantify any meaningful temporal gravity change related to the postseismic process. An alternate and better approach is to decompose the gravity field data into moment tensor components, as used in Han *et al.* [2013, 2014].

3. Normal Mode Decomposition of Gravity Data

Coseismic and postseismic changes in Earth's gravitational field result from a combination of volumetric strain (producing change in the Lagrangian density) and redistribution of mass through static and quasi-static displacements, particularly vertical motions across discontinuities in reference density. According to Kanamori and Given [1981] and Pollitz [1997], the gravity and displacement time series at each location is computed by linear combination of the changes (eigenmodes) corresponding to five independent moment tensor components of M_{rr} , $M_{r\theta}$, $M_{r\varphi}$, $M_{\theta\theta} - M_{\varphi\varphi}$, and $M_{\theta\varphi}$ (r for radius, θ for colatitude, and φ for longitude). Following the procedures of normal mode decomposition and spatial localization used in Han *et al.* [2014] for the 2011 Tohoku-Oki earthquake analysis, we computed the spatial patterns and the respective time series of GRACE gravity observations in terms of the earthquake moment change. For

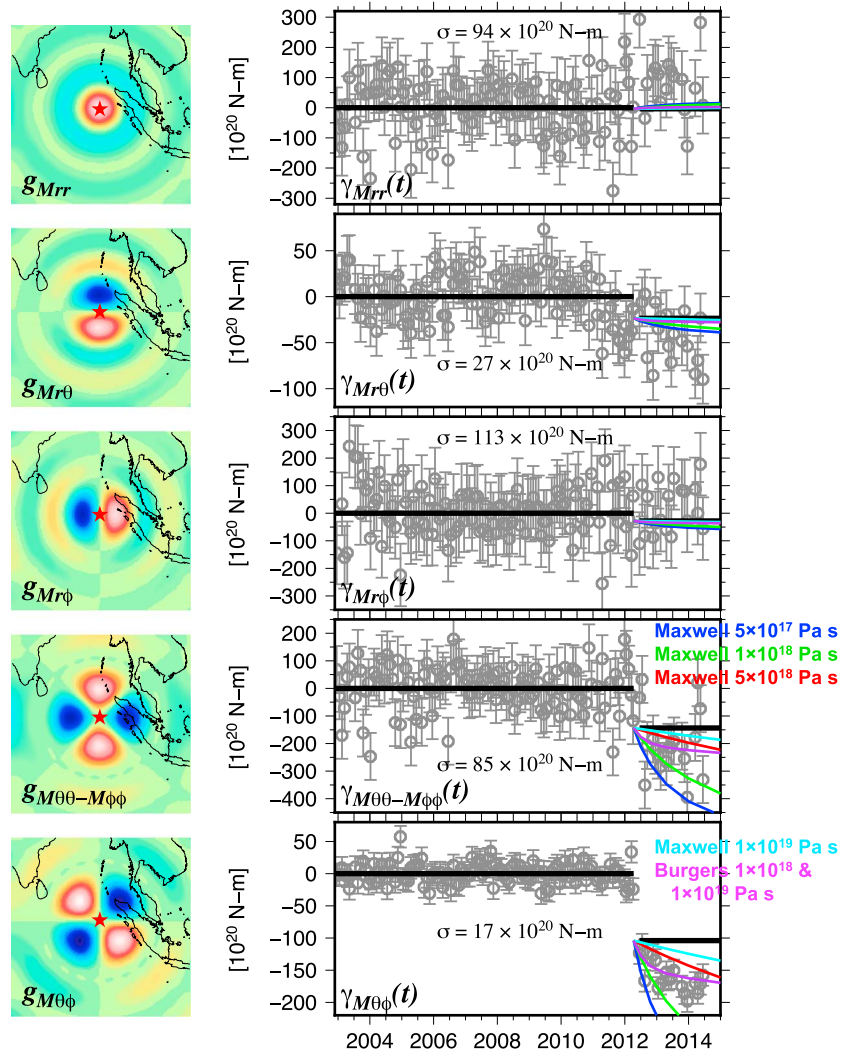


Figure 3. (left column) The predicted spatial patterns of the gravity changes to be excited by five independent moment tensor components of M_{rr} , $M_{r\theta}$, $M_{r\phi}$, $M_{\theta\theta} - M_{\phi\phi}$, and $M_{\theta\phi}$, respectively. The exact scale is dependent on the moment tensor (the negative to positive values are depicted with blue to red colors). The average coordinate of the finite fault sources is 1.8°N , 92.3°E (depicted as a red star) and the depth is 30 km. (right column) The corresponding temporal variations of each component of the gravity change before and after the earthquake. The GRACE observations are shown by gray circles with the error estimates. The synthetic gravity changes computed from the finite fault model are shown in thick black solid line. The depicted postseismic viscoelastic gravity changes computed from the Maxwell asthenosphere model with the viscosity of 5×10^{17} Pa s (blue), 10^{18} Pa s (green), 5×10^{18} Pa s (red), and 10^{19} Pa s (cyan) and from the biviscous (Burgers body) asthenosphere model with transient viscosity of 10^{18} Pa s and steady state viscosity of 10^{19} Pa s (purple). Note the mathematical expressions of the gravity spatial pattern g_M and the associated temporal pattern $\gamma_M(t)$ were defined in Han et al. [2014].

these earthquake mechanisms, GRACE resolves the gravity changes associated with $M_{r\theta}$ and $M_{\theta\phi}$ components several times better than the other components of M_{rr} , $M_{r\phi}$ and $M_{\theta\theta} - M_{\phi\phi}$ due to the sampling nature of intersatellite ranging between two spacecraft in the near-polar orbit [Han et al., 2013, 2014]. Therefore, the data noise at a fixed spatial location would be dominated by errors in the observed gravity changes corresponding to M_{rr} , $M_{r\phi}$ and $M_{\theta\theta} - M_{\phi\phi}$.

The spatial patterns of the gravity changes corresponding to M_{rr} , $M_{r\theta}$, $M_{r\phi}$, $M_{\theta\theta} - M_{\phi\phi}$ and $M_{\theta\phi}$ are shown in Figure 3 (left column). We used a depth of 30 km for the centroid from Duputel et al. [2012]. As discussed in Han et al. [2013], the isotropic (monopole) gravity change is particularly sensitive to the centroid depth (precisely speaking, the bulk modulus at the centroid location). The GRACE time series of the respective

moment estimates are shown next to the spatial map in Figure 3 (see the supplementary material of Han *et al.* [2014] for the mathematical detail). Each time series was detrended by removing the effect of seasonal climate signal and of the 2004 Sumatra-Andaman earthquake, as we discussed in section 2. The original GRACE data and the data fit are shown in the supporting information Figure S1. The error bar (σ) for each component was estimated from the difference between the GRACE data and the fit up to March of 2012 (before the earthquake). We found the errors as large as $85\text{--}113 \times 10^{20}$ N m (M_w 8.6–8.7) for the component of M_{rr} , $M_{r\phi}$, and $M_{\theta\theta} - M_{\phi\phi}$, 27×10^{20} N m (M_w 8.3) for $M_{r\theta}$, and 17×10^{20} N m (M_w 8.2) for $M_{\theta\phi}$. It demonstrates that the GRACE data are suitable for analyzing strike-slip earthquakes as small as M_w 8.2 in this region.

If the Earth were purely elastic, the time series of each moment change (such as Figure 3) would have been those of a Heaviside step function with the episodic change at the earthquake occurrence time. Any deviation from the step function would be the result of GRACE data noise, the effect of viscoelastic earth, postseismic slip, and/or some other postseismic processes. From Duputel *et al.* [2012], combining M_w 8.6 main shock and M_w 8.2 aftershock, we obtain the coseismic moment; $M_{rr} = -6 \times 10^{20}$ N m, $M_{r\theta} = -17 \times 10^{20}$ N m, $M_{r\phi} = -21 \times 10^{20}$ N m, $M_{\theta\theta} - M_{\phi\phi} = -154 \times 10^{20}$ N m, and $M_{\theta\phi} = -115 \times 10^{20}$ N m. The corresponding coseismic offset for each component is in good agreement with the estimates from the finite fault model of the main shock from Yue *et al.* [2012], when scaled up by 1.2 to account for the aftershock and approximated and decomposed into a point-source double couple, which are shown as thick black solid lines in Figure 3. The other model from Wei *et al.* [2013] is not significantly different from these. The GRACE data resolve the episodic gravity change associated with $M_{\theta\theta} - M_{\phi\phi}$ to be $-154 \pm 85 \times 10^{20}$ N m and the one with $M_{\theta\phi}$ to be $-105 \pm 17 \times 10^{20}$ N m and indicate no significant changes in the other components given the associated data noise. It is the $M_{\theta\phi}$ component that shows the largest gravity signal with the smallest data noise with the signal-to-noise ratio greater than 5. The GRACE data in $M_{\theta\phi}$ imply also significant postseismic changes with a magnitude of 60–70% of the coseismic perturbation only in 2–3 years.

4. Viscoelastic Relaxation Model

The observed large reduction of shear wave velocity at the lithosphere-asthenosphere boundary has been hypothesized to be due to a partially molten asthenosphere consisting of horizontal melt-rich layers embedded in a meltless mantle [Kawakatsu *et al.*, 2009]. Consistent with this interpretation, we found that viscoelastic relaxation within the low viscosity asthenosphere was a dominant process that governed regional-scale deformation and postseismic gravity change observed persistently after the 2004 Sumatra-Andaman and the 2011 Tohoku-Oki earthquakes [Han *et al.*, 2008, 2014]. Here we model the gravity change with alternate viscoelastic relaxation models to understand the postseismic change evident particularly in the time series of the $M_{\theta\phi}$ component after the 2012 Indian Ocean earthquakes.

As noted earlier, the moment release as a function of depth from the seismological solution for the 2012 earthquake sequence [e.g., Wei *et al.*, 2013] indicates the highest moment release occurred at 40 km depth at the point of the maximum predicted differential stress and highest rigidity, and the moment release tapers to zero from 40 to 60 km. We used a spherically stratified viscoelastic Earth model that includes a global ocean layer (3 km thick) on top of the elastic lithosphere (60 km thick), the asthenosphere (63–220 km), and an upper (220–670 km) and lower (670–2891 km) mantle. An elastic lithosphere was approximated by making the viscosity very large (10^{30} Pa s). The upper and lower mantle were modeled with a Maxwell rheology with the viscosity of 10^{20} Pa s and 10^{21} Pa s, respectively.

For the asthenosphere, we tested five different rheological models (1) Maxwell viscosity of 5×10^{17} Pa s, (2) 10^{18} Pa s, (3) 5×10^{18} Pa s, (4) 10^{19} Pa s, and finally (5) transient (Kelvin) viscosity of 10^{18} Pa s and steady state (Maxwell) viscosity of 10^{19} Pa s with biviscous (Burgers body) rheology. As in our previous analysis for the 2004 and 2011 events, we used the computer code VISCO1D for testing alternate spherical viscoelastic models [Pollitz, 1997; Pollitz *et al.*, 2006] to compute the displacement and gravity changes at the surface.

The computed gravity changes from five different cases of the asthenospheric viscosity are shown in the solid colored lines of Figure 3. The viscoelastic gravity changes in the monopole and dipole components are small since the moment release in these components is 1 order of magnitude smaller than those in the quadruple

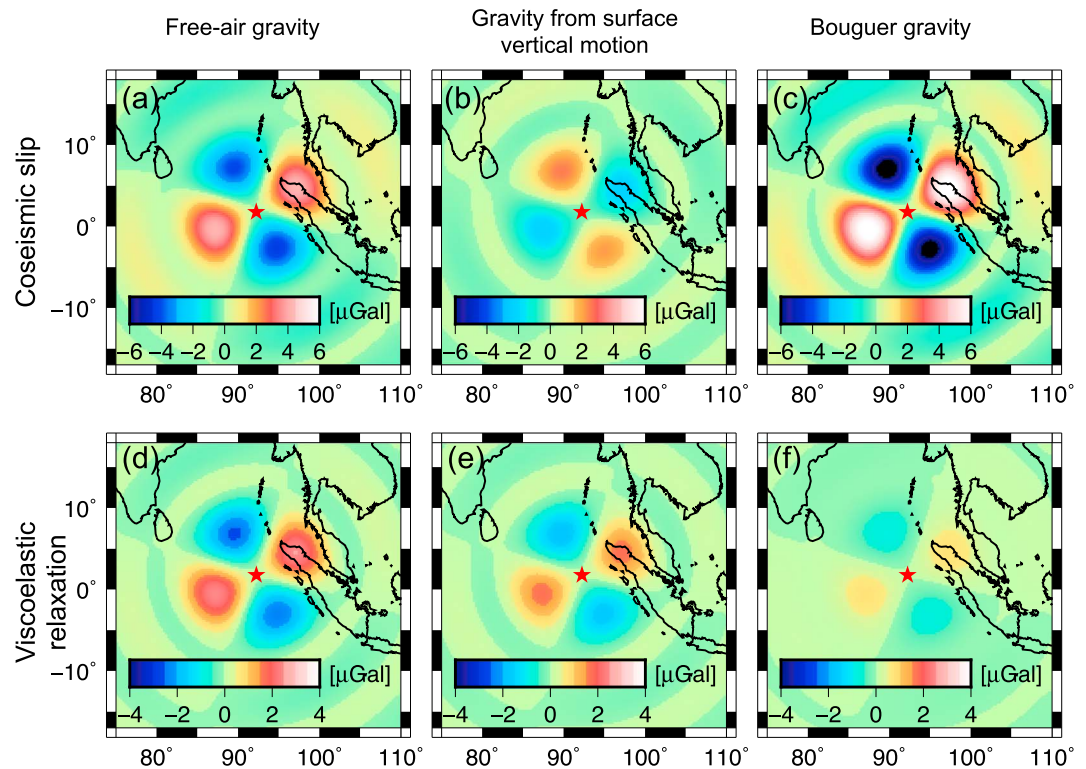


Figure 4. The (top) coseismic and (bottom) postseismic synthetic gravity changes of elastic deformation and viscoelastic relaxation computed with the finite fault model and the biviscous viscoelastic relaxation model. The free-air, surface vertical motion-induced, and Bouguer gravity changes were computed separately to highlight the distinct surface (change in seafloor height) and interior (bulk density change) sources of deformation. The viscoelastic gravity computations are snapshots at the beginning of year 2014.

components. While the observations of the quadruple component, $M_{\theta\theta} - M_{\phi\phi}$, are too noisy to distinguish any difference among various models, the $M_{\theta\phi}$ observations are accurate enough to discriminate the biviscous rheology from the various Maxwell cases and to infer a lower transient viscosity of 10^{18} Pa s and larger steady state viscosity of 10^{19} Pa s. We also found that the depth of the asthenosphere generally compensates with the magnitude of viscosity, for example, a 10 km shallower asthenosphere demands 10–20% larger viscosity to fit the data.

5. Discussion and Conclusions

Both the GRACE data and the viscoelastic model based on it indicate a postseismic gravity change of $\pm 3 \mu\text{Gal}$ in 2 years, which is nearly 60% of the coseismic gravity change of $\pm 5 \mu\text{Gal}$ with similar spatial patterns of the gravity changes, as shown in free-air gravity maps of Figures 4a (coseismic) and 4d (postseismic), respectively. The gravity change is a manifestation of vertical displacement of any density interface (e.g., seafloor and Moho) and of interior deformation (compression and dilatation).

For coseismic (elastic) deformation, the seafloor in the compressional quadrant underwent subsidence, which caused the negative gravity change. The seafloor vertical motion causes gravity change by $0.7 \mu\text{Gal}$ per 1 cm of uplift that is the Bouguer correction, $2\pi G(\rho_c - \rho_w)h$, where G is the gravitational constant, ρ_c is the seafloor (upper crust) density, ρ_w is the ocean density, and h is the vertical displacement of the seafloor. However, the effect of compression yielding the positive gravity change was so large as to overcome the negative gravity change induced by surface depression, as shown in the Bouguer gravity of Figure 4c, and, ultimately, resulted in the positive free-air gravity in the compressional quadrant. The Bouguer gravity (indicating the amount of compression) is essentially controlled by the bulk modulus at seismic source [Han et al., 2013]. Similarly, the gravity change in the dilatational quadrant can be explained, namely, the gravity effect due to the interior dilatation (the negative

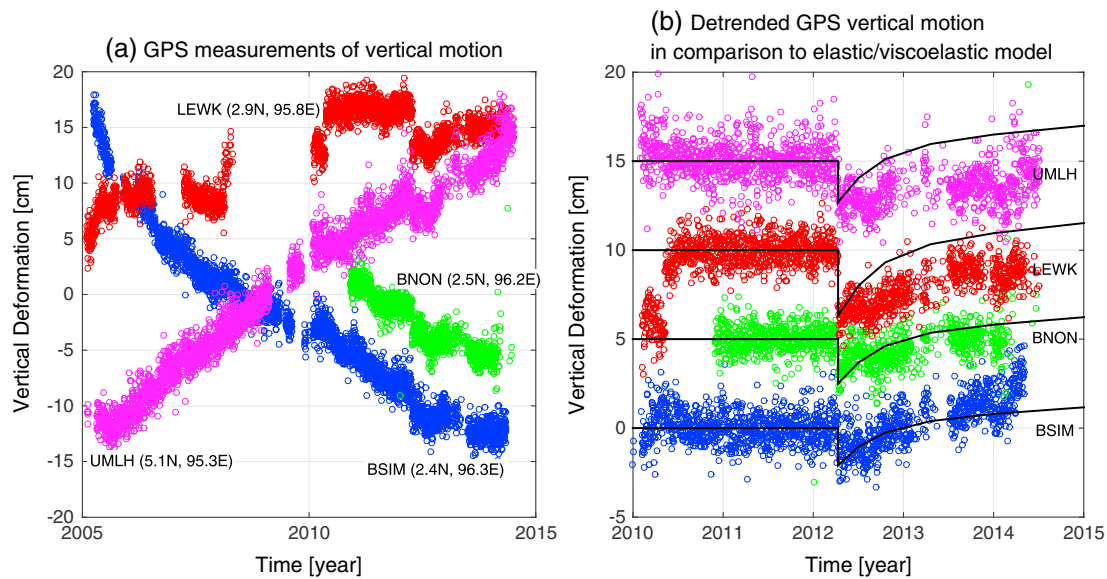


Figure 5. (a) Daily GPS observations of vertical deformation at the GPS sites. UMLH locates at the Aceh region while BSIM, BNON, and LEWK are at the Simeulue island. (b) The detrended GPS time series, the linear trend, and seasonal components were estimated using the data from year 2010.5 to 2012.275 (before the great 2012 earthquakes) and removed from the data after 2012.275. Therefore, the detrended data highlight the vertical motion relative to the average motion during the period from 2010.5 to 2012.275. The solid black line shows the synthetic vertical motion computed with the coseismic and viscoelastic models used in Figure 4 compared to the GPS data.

Bouguer gravity) was larger than the positive gravity caused by the coseismic seafloor uplift, thus yielding the negative free-air gravity.

The deformation associated with postseismic viscoelastic relaxation is completely different from the coseismic deformation although their free-air gravity patterns are similar. First, the postseismic seafloor displacement is uplift in the compressional quadrant unlike the coseismic seafloor motion (Figure 4e). Second, not only the seafloor but also other density interfaces such as the Moho are uplifted in the compressional quadrant and subsided in the dilatational quadrant postseismically without significant perturbation in density. It is the postseismic vertical motion, rather than density change, that results in the positive and negative Bouguer gravity changes in the compressional and dilatational quadrants, respectively (Figure 4f). The deformation is, in general, far more complex near the faults, as indicated by the higher-resolution computation (up to ~55 km) shown in Figure S2. However, in the far field where most of GPS stations are located (Simeulue island and Aceh; see Figure 1), the deformation is consistent with GRACE observations at a spatial scale of 500 km.

We also examined the GPS vertical motion in association with the 2012 earthquakes. The four nearby stations to the strike-slip faults were chosen where the largest coseismic motions were detected. Figure 5a shows the time series of vertical motion at GPS stations of BSIM, BNON, and LEWK on the Simeulue island and UMLH on the Aceh. The prolonged long-term trends are evident in the original vertical data over the 10 years (2005–2014) that are likely primarily due to postseismic deformation from the 2004 Sumatra-Andaman and 2005 Nias megathrust events and interseismic deformation as well as other moderate and large earthquakes. We used the data from 2010.5 (after the major motion in LEWK) to 2012.275 (before the 2012 earthquakes) to determine the linear trend and seasonal components. We removed these signals from the GPS data after 2012.275 to highlight the signals only related to the 2012 ruptures. In Figure 5b, all stations show episodic (coseismic) subsidence and gradual (postseismic) uplift, when highlighted with respect to the motion during 2010.5–2012.275. The overall trends of GPS vertical motions are consistent with the elastic and biviscous relaxation models of the 2012 earthquakes with the viscosity constrained solely by GRACE data, as shown in black solid lines indicating the high-resolution VISCO1D and STATIC1D model runs at each GPS location. However, differences also exist due to coseismic and postseismic effects from numerous other smaller events before and after the 2012 ruptures.

All GPS stations are located within the compressional quadrant, where GRACE observed positive gravity change both coseismically and postseismically. The coseismic positive gravity from GRACE and the coseismic subsidence from GPS are the result of spontaneous compression, and thus density increase in the compressional quadrant. The postseismic positive gravity from GRACE and the postseismic uplift from GPS are due to the gradual uplift associated with viscoelastic relaxation with little perturbation in density. Afterslip on or near to the Indian Ocean earthquake fault planes is unlikely to be the dominant postseismic process for this earthquake because the associated far-field deformation is expected to mimic the coseismic deformation field. That is, in the compressional quadrant, afterslip would result in a positive gravity change but a negative vertical motion, contrary to the GPS observations of postseismic uplift (Figure 5b). In continental [e.g., *Savage et al.*, 2007; *Cattania et al.*, 2015] and megathrust [*Lange et al.*, 2014] settings, afterslip is thought to be highly correlated with aftershock rates. The few aftershocks of the M_w 8.6 11 April 2012 earthquake in comparison with the aftershocks from other megathrusts of the same magnitude [*Shcherbakov et al.*, 2013] may also be indicative of lack of substantial afterslip.

In addition to the recent great megathrust ruptures in 2004, 2010, and 2011, this earthquake is a rare example from which we can advance our understanding on the Earth's response to these large episodic stress changes under different environments by testing various hypotheses and physics of postseismic processes. Deciphering the roles of viscoelastic relaxation, postseismic slip ("afterslip"), and poroelastic relaxation (not discussed here) are crucial in order to infer the redistribution of stress at or near the subduction boundary and to understand the interseismic stress loading cycle, and thus to assess seismic hazards [*Hetland and Hager*, 2006]. Continuous GRACE observations of these postseismic deformation processes provide fundamental quantification of the large-scale rheological behavior of the solid Earth.

Acknowledgments

The GRACE data used in this paper are available at <http://podaac.jpl.nasa.gov/GRACE>. The time series of GPS positions were processed by Nevada Geodetic Laboratory and available from <http://cheryl.nbnmg.unr.edu>. We thank DLR for providing the GRACE telemetry data and JPL, CSR, and GFZ for producing the high-quality Level 1B and Level 2 products. The Earth Observatory of Singapore is acknowledged for designing, deploying, and maintaining the Sumatran GPS Array (SuGAR). Reviews of the manuscript by J. Savage and Eileen Evans, the Editor, and two anonymous reviewers are greatly appreciated.

The Editor thanks two anonymous reviewers for their assistance in evaluating this paper.

References

- Cattania, C., S. Hainzl, L. Wang, B. Enescu, and F. Roth (2015), Aftershock triggering by postseismic stresses: A study based on Coulomb rate-and-state models, *J. Geophys. Res. Solid Earth*, *120*, doi:10.1002/2014JB011500.
- Delescluse, M., N. Chamot-Rooke, R. Cattin, L. Fleitout, O. Trubienko, and C. Vigny (2012), April 2012 intra-oceanic seismicity off Sumatra boosted by the Banda-Aceh megathrust, *Nature*, *490*(7419), 240–244.
- Duputel, Z., H. Kanamori, V. C. Tsai, L. Rivera, and L. Meng (2012), The 2012 Sumatra great earthquake sequence, *Earth Planet. Sci. Lett.*, *351–352*, 247–257.
- Han, S.-C., J. Sauber, S. B. Luthcke, C. Ji, and F. F. Pollitz (2008), Implications of postseismic gravity change following the great 2004 Sumatra-Andaman earthquake from the regional harmonic analysis of GRACE intersatellite tracking data, *J. Geophys. Res.*, *113*, B11413, doi:10.1029/2008JB005705.
- Han, S.-C., R. Riva, J. Sauber, and E. Okal (2013), Source parameter inversion for recent great earthquakes from a decade-long observation of global gravity fields, *J. Geophys. Res. Solid Earth*, *118*, 1240–1267, doi:10.1002/jgrb.50116.
- Han, S.-C., J. Sauber, and F. Pollitz (2014), Broad-scale postseismic gravity change following the 2011 Tohoku-Oki earthquake and implication for deformation by viscoelastic relaxation and afterslip, *Geophys. Res. Lett.*, *41*, 5797–5805, doi:10.1002/2014GL060905.
- Hetland, E. A., and B. H. Hager (2006), The effects of rheological layering on post-seismic deformation, *Geophys. J. Int.*, *166*, 277–292.
- Hill, E. M., et al. (2015), The 2012 M_w 8.6 Wharton Basin sequence: A cascade of great earthquakes generated by near-orthogonal, young, oceanic-mantle faults, *J. Geophys. Res. Solid Earth*, doi:10.1002/2014JB011703.
- Kanamori, H., and J. W. Given (1981), Use of long-period surface waves for rapid determination of earthquake source parameters, *Phys. Earth Planet. Inter.*, *27*, 8–31.
- Kawakatsu, H., P. Kumar, Y. Takei, M. Shinohara, T. Kanazawa, E. Araki, and K. Suyehiro (2009), Seismic evidence for sharp lithosphere-asthenosphere boundaries of oceanic plates, *Science*, *324*, 499–502.
- Lange, D., J. R. Bedford, M. Moreno, F. Tilmann, J. C. Baez, M. Bevis, and F. Krüger (2014), Comparison of postseismic afterslip models with aftershock seismicity for three subduction-zone earthquakes: Nias 2005, Maule 2010 and Tohoku 2011, *Geophys. J. Int.*, *199*, 784–799.
- McGuire, J., and G. Beroza (2012), A rogue earthquake off Sumatra, *Sci. Express*, *336*, doi:10.1126/science.1223983.
- Meng, L., J.-P. Ampuero, J. Stock, Z. Duputel, Y. Luo, and V. C. Tsai (2012), Earthquake in a maze, compressional rupture branching during the 2012 M_w 8.5 Sumatra earthquake, *Science*, *337*, 10 August 2012.
- Pollitz, F., R. S. Stein, V. Sevilgen, and R. Burgmann (2012), The 11 April 2012 east Indian Ocean earthquake trigger large aftershocks worldwide, *Nature*, *490*, 250–253.
- Pollitz, F., R. Burgmann, R. S. Stein, and V. Sevilgen (2014), The profound reach of the 11 April 2012 $M_8.6$ Indian Ocean earthquake: Short-term global triggering following by a longer-term global shadow, *Bull. Seismol. Soc. Am.*, *104*(2), 972–984, doi:10.1785/0120130078.
- Pollitz, F. F. (1997), Gravitational viscoelastic postseismic relaxation on a layered spherical Earth, *J. Geophys. Res.*, *102*, 17,921–17,941, doi:10.1029/97JB01277.
- Pollitz, F. F., P. Banerjee, R. Bürgmann, M. Hashimoto, and N. Choosakul (2006), Stress changes along the Sunda trench following the 26 December 2004 Sumatra-Andaman and 28 March 2005 Nias earthquakes, *Geophys. Res. Lett.*, *33*, L06309, doi:10.1029/2005GL024558.
- Rollins, J. C., and R. S. Stein (2010), Coulomb stress interactions among $M > 5.9$ earthquakes in the Gorda deformation zone and on the Mendocino Fault Zone, Cascadia subduction zone, and northern San Andreas fault, *J. Geophys. Res.*, *115*, B12306, doi:10.1029/2009JB007117.
- Savage, J. C., J. L. Svarc, and S.-B. Yu (2007), Postseismic relaxation and aftershocks, *J. Geophys. Res.*, *112*, B06406, doi:10.1029/2006JB004584.

- Shcherbakov, R., K. Goda, A. Iwanian, and G. Atkinson (2013), Aftershock statistics of major subduction earthquakes, *Bull. Seismol. Soc. Am.*, *103*, 3222–3234, doi:10.1785/0120120337.
- Tapley, B. D., S. Bettadpur, J. Ries, P. Thompson, and M. Watson (2004), GRACE measurements of mass variability in the Earth system, *Science*, *305*, 503–505, doi:10.1126/science.1099192.
- Wei, S., D. Helmberger, and J. P. Avouac (2013), Modeling the 2012 Wharton basin earthquakes off-Sumatra: Complete lithospheric failure, *J. Geophys. Res. Solid Earth*, *118*, 3592–3609, doi:10.1002/jgrb50267.
- Yue, H., T. Lay, and K. Koper (2012), En echelon and orthogonal fault ruptures of the 11 April 2012 great intraplate earthquakes, *Nature*, *490*(7419), 245–249.